

High Conducting Nanowires Obtained From Uniform Titanium Covered Carbon Nanotubes

Sefa DAĞ, Engin DURGUN and Salim ÇIRACI

*Department of Physics, Bilkent University,
Bilkent, Ankara 06800, TURKEY*

Received 11.10.2005

Abstract

We have shown that Ti atoms can form continuous coating of carbon nanotubes at different amount of coverage. The circular cross section changes to a square-like form, and the semiconducting tube becomes ferromagnetic metal with high quantum ballistic conductance. Metallicity is induced not only by the metal-metal coupling, but also by the band gap closing of SWNT at the corners of the square. The magnetic properties of Ti coated tubes depend strongly on the geometry, amount of Ti coverage and also on the elastic deformation of the tube. While the magnetic moment can be pronounced significantly by the positive axial strain, it can decrease dramatically upon the adsorption of additional Ti atoms to those already covering the nanotube. Besides, electronic structure and spin-polarization near the Fermi level can also be modified by radial strain. Our results have been obtained by the first-principles, spin-relaxed pseudopotential plane wave calculations within the density functional theory.

Key Words: carbon nanotube, titanium, nanowire, first principles, ab initio

1. Introduction

The fabrication of interconnects with high conductance and low energy dissipation has been a real challenge in rapidly developing field of nanoelectronics. Very thin metal wires and atomic chains have been produced by retracting the STM tip from an indentation and then by thinning the neck of the materials that wets the tip [1, 2, 3]. While those nanowires produced so far played a crucial role in understanding the quantum effects in electronic and thermal conductance [4, 5, 6], they were neither stable nor reproducible to offer any relevant application. It has been shown that SWNTs can serve as templates to produce reproducible, very thin metallic wires with controllable sizes [7]. Continuous Ti coating of varying thickness, and quasi continuous coating of Ni and Pd were obtained by using electron beam evaporation techniques [8]. Good conductors, such as Au, Al, were able to form only isolated discrete particles or clusters instead of a continuous coating of SWNT. Low resistance ohmic contacts to metallic and semiconducting SWNTs have been achieved also by Ti and Ni atoms [9]. In spite of the impact made by these experimental works [7, 8, 9] there has been very little effort so far to present an atomic scale understanding of uniform Ti coverage.

In this paper we show that a semiconducting s-SWNT is transformed to a good conductor as a result of Ti coverage. The circular cross section changes to a square-like form. Moreover, Ti covered tubes have magnetic ground state with a net magnetic moment. We investigate how the magnetic moment μ , and spin polarization ($P(E_F)$) can be modified with the applied strain and amount of Ti coverage. We found that μ , as well as $P(E_F)$ depend strongly on the applied strain and on the Ti coverage. While a strain of $\epsilon_{zz} = 0.1$ along the axis of the tube induces 25% increase of μ , the adsorption of four additional Ti atoms on the Ti coated (8,0) SWNT, causes to 44% reduction of the magnetic moment. The radial strain leading to the elliptical deformation of the circular cross section modifies the spin-dependent electronic structure

near E_F . The manipulation of spin-dependent properties of Ti coated SWNT with applied strain and with Ti coverage suggest interesting technological applications such as spin filter, spin-resonant-tunnelling diode, unipolar spin transistor and nanoscale magnetism, *etc.*

These results have important implications in nanoscience and nanotechnology.

2. Method

We performed spin-relaxed, first-principles pseudopotential plane wave calculations [10, 11] within density functional theory [12]. We used spin-polarized generalized gradient approximation (GGSA) [13] and ultrasoft pseudopotential [11, 14] with a uniform energy cutoff 300 eV. Calculations have been performed in momentum space by using periodically repeating tetragonal supercell with lattice constants, $a_s = b_s \sim 20 \text{ \AA}$ and $c_s = c$ (c being the one-dimensional (1D) lattice constant of SWNT). The Brillouin zone of the supercell is sampled by using Monkhorst-Pack [15] special \mathbf{k} -point scheme. All atomic positions (*i.e.* all adsorbed Ti atoms and carbon atoms of SWNT), as well as c_s have been optimized. In order to further test that the structures of Ti adsorbed or Ti coated SWNTs obtained through geometry optimization are stable we carried out *ab initio* molecular dynamics calculations at $T = 500 \text{ K}$ using Nosé thermostat. All structures reported in this work are maintained stable at $T = 500 \text{ K}$ for sufficient number of time steps.

3. Ti coverage

The (8,0) zigzag tube is a semiconductor, the band gap of which has been calculated to be, $E_g = 0.6 \text{ eV}$. An individual Ti atom is adsorbed at specific sites on the external and internal surface of SWNT. The H-site, *i.e.* above the center of hexagon formed by C-C bonds, is found to be energetically most favorable site with a binding energy of $E_b = 2.2 \text{ eV}$ for the magnetic ground state. The average C-Ti distance, \bar{d}_{C-Ti} has been found to be 2.2 \AA . At the internal H-site, the bonding is stronger and the binding energy is $E_b = 2.5 \text{ eV}$, the average bond distance $\bar{d}_{C-Ti} = 2.3 \text{ \AA}$. The magnetic moment of the individual Ti adsorbed (8,0) SWNT is calculated to be $\mu = 2.2\mu_B$ (Bohr magneton). Ti $3d$ -orbitals play a crucial role in the bonding and electrons are transferred from Ti to SWNT [16].

A strong Ti-SWNT chemical interaction is responsible for the continuous coating. Here, the Ti coverage of (8,0) SWNT has been analyzed first by attaching Ti atoms at all H-sites in the unit cell, and subsequently by optimizing the atomic structure and the lattice constant c . The relaxation of the SWNT lattice was crucial in obtaining stable structures; frozen lattice constant has led to instabilities. The average binding energy, $\bar{E}_b = (16E_T[Ti] + E_T[SWNT] - E_T[16Ti + SWNT])/16$, has been found (in terms of the total energies of individual Ti atom, optimized bare SWNT and Ti covered SWNT) to be 4.3 eV . Apparently, owing to the Ti-Ti coupling, \bar{E}_b comes out much higher than the binding energy of the adsorbed single Ti atom. For the same reason the charge transfer from Ti to C has decreased to ~ 0.3 electrons, and \bar{d}_{C-Ti} increased to $\sim 2.5 \text{ \AA}$.

The optimized atomic structure shown in Figure 1 depicts an interesting feature of the Ti covered SWNT. Atoms have rearranged in a quasi 1D "crystalline" structure and formed a square-like cross section. We distinguish three specific C atoms (identified as C1, C2, and C3) and three Ti atoms (Ti1, Ti2 and Ti3) depending on their different bonding geometry. The C1 and Ti1 atoms located at the corner of square are at the high curvature site, while C3 and Ti3 are at the flat region. In spite of the periodic arrangement of adsorbed Ti and underlying C atoms, the Ti-Ti, Ti-C, and C-C bond-distances show some dispersion depending on their location. The histogram in Figure 1 identifies different types of bonds at different places.

The energy band structure and the total density of states (TDOS) of the Ti covered (8,0) SWNT are presented in Figure 2. The band structure of the bare semiconducting (8,0) SWNT has changed dramatically having several bands crossing the Fermi level. Accordingly, the Ti covered SWNT becomes a good conductor with high density of states at the Fermi level, $\mathcal{D}(E_F)$. The current associated with the electron transport can be given by a Landauer type expression [17],

$$I(V_b) = \frac{2e^2}{h} \int_{\mu_r}^{\mu_l} dE (f_l - f_r) \mathcal{T}(E, V_b) dE \quad (1)$$

in terms of the bias voltage V_b ; the Fermi distribution function of left and right electrodes f_l and f_r , and their chemical potentials μ_l and μ_r . Electron scattering in the contacts is crucial for the calculation of conductance. Therefore, the calculation of quantum conductance \mathbf{G} of an interconnect between two electrodes requires detailed description of the contacts and phonon spectrum at the operation temperature. Here, since we are concerned only with the nanowire, we infer \mathbf{G} from an ideal Ti covered SWNT. Under these circumstances, the mean free path of electrons l_m becomes infinite at $T=0$, and the electronic transport occurs ballistically and coherently. This situation has been treated as an ideal 1D constriction, where the electrons are confined in the transversal direction, but propagate freely along the axis [5]. The current is expressed as $I = \sum_i 2\eta_i e v_i [\mathcal{D}_i(E_F + eV_b) - \mathcal{D}_i(E_F)]$ where degeneracy, group velocity and density of states of each subband crossing E_F are given by η_i , v_i , \mathcal{D}_i , respectively. Since $\mathcal{D}_i(E_F + eV_b) - \mathcal{D}_i(E_F) \sim (eV_b)d\mathcal{D}_i(E)/dE|_{E_F}$ and $v_i = (\hbar^{-1})\partial\mathcal{D}_i/\partial E|_{E_F}$, then $G = I/V_b = \sum_i 2\eta_i e^2/h$. Accordingly each subband crossing the Fermi level is counted as η_i current-carrying state for two spins with channel transmission $\mathcal{T} = 1$. Then the maximum "ideal" conductance of defect-free Ti covered ideal tube becomes $G = 2e^2 N_b/h$, where $N_b = \sum \eta_i$. Calculated conductance is four times higher than that of bare metallic armchair tube. This situation is apparent by high $\mathcal{D}(E_F)$ in Figure 2.

In reality, $\mathcal{T}(E)$ in Eq. 1 is reduced due to scattering of carriers from the abrupt change of cross sections and irregularities at the contacts to electrodes and from the imperfections, impurities, and electron-phonon scattering in the tube by itself. We note that the regular structure shown in Figure 1 may occur under idealized conditions; normally irregularities are unavoidable, in particular for a thick Ti coating. While the channel transmission is decreased in the thick but inhomogeneous Ti coating, \mathbf{G} is expected to be still high owing to the new conductance channels opened at E_F . Based on these arguments and in view of the high $\mathcal{D}(E_F)$ in Figure 2, the conductance of a Ti coated tube can be several $2e^2/h$.

Any defect in 1D system gives rise to the localization of current transporting states which is characterized by the localization length ξ . While $\xi \sim l_m$ for a strictly 1D wire, $\xi \sim l_m d/\lambda_F$ for a 1D stripe and $\xi \sim l_m d^2/\lambda_F^2$ for a wire with width or diameter d and Fermi wavelength, $\lambda_F = \hbar/mv_F$ [18]. We expect that for the present Ti covered SWNT $\xi \sim l_m(d/\lambda_F)^\alpha$ with $1 < \alpha < 2$. Then the net resistance of (Ti+SWNT) wire having length L between two contact and including contact resistance R_c and localization effect can be given by $R = R_c + \hbar e^{L/\xi}/2e^2$. A crude estimation yields $\xi \geq 200\text{\AA}$, which is much larger than a typical L for interconnects in nanoelectronics.

The origin of metallicity is the next question we will address. First, let us consider the nanotube having the same atomic configuration, hence the same square-like cross section as in Figure 1, but depleted from all adsorbed Ti atoms. The local densities of states (LDOS) at C1, C2, and C3 carbon atoms in Figure 3(a) clarify whether such a deformed SWNT continues to be semiconducting. For the atom C3, which is located at the center of the edge of square, *i.e.* at the flat region of the tube the state density vanishes at E_F . In contrast, as one approaches the corner, LDOS at E_F increases, and eventually at C1 (*i.e.* the atom at the corner of the square) has the highest density. This situation implies that the square nanotube by itself (without Ti) can be viewed as if four metal strips passing through its four corners, and four semiconductors at the flat edges. The metallization is induced by the singlet conduction band that crossed the Fermi level due to enhanced $\pi^* - \sigma^*$ hybridization at the corner region in Figure 3(a) and 3(b) [19, 20, 21]. In Figure 3(c), the LDOS and orbital projected LDOS calculated at Ti atoms have high state density at E_F due to the states derived mainly from Ti $3d$ -orbitals. Accordingly, the main contribution to the high $\mathcal{D}(E_F)$ in Figure 2 is due to adsorbed Ti atoms, but the underlying carbon tube itself has some contribution.

Uniform coverage of Ti on the SWNT is crucial for the future technological applications. Ti can be used as a buffer layer to form uniform coating of good conductors, such as Au, Cu, on the SWNT [16], since these atoms have low binding energy (0.5 and 0.7 eV, respectively). Strong Ti-SWNT interaction can be utilized to bond or to connect individual SWNTs in order to form T, Y and cross junctions or grids. It appears that fabrication of photonic band gap materials or nano-waveguide based on SWNT may not be a mere speculation. Earlier, it has been shown that quantum structures can be realized on a single s-SWNT through band gap modulation either by modulating radial deformation or by modulating adsorption of hydrogen atoms [20, 22]. These quantum structures can be connected to the electrodes through their both ends which are metallized by Ti coverage. This way one can fabricate an electronic nanodevice on a single SWNT, such as a Schottky barrier diode or a resonant tunnelling device.

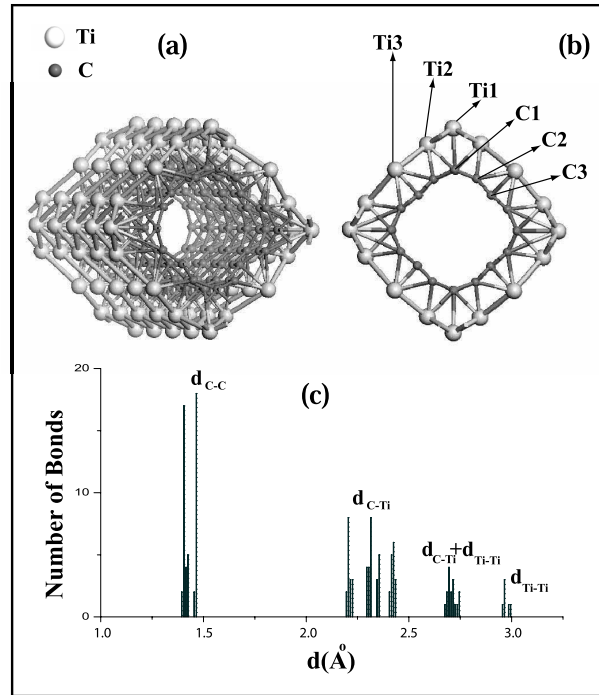


Figure 1. (a) Fully optimized atomic structure of Ti covered (8,0) SWNT. (b) The cross section with different types of C atoms (identified as C1, C2, and C3) and adsorbed Ti atoms (Ti1, Ti2 and Ti3). Dark-small and light-large circles indicate C and Ti atoms, respectively. (c) Histograms show the variation of bond-lengths of different carbon-carbon (\bar{d}_{C-C}), carbon-Ti (\bar{d}_{C-Ti}) and Ti-Ti (\bar{d}_{Ti-Ti}) bonds.

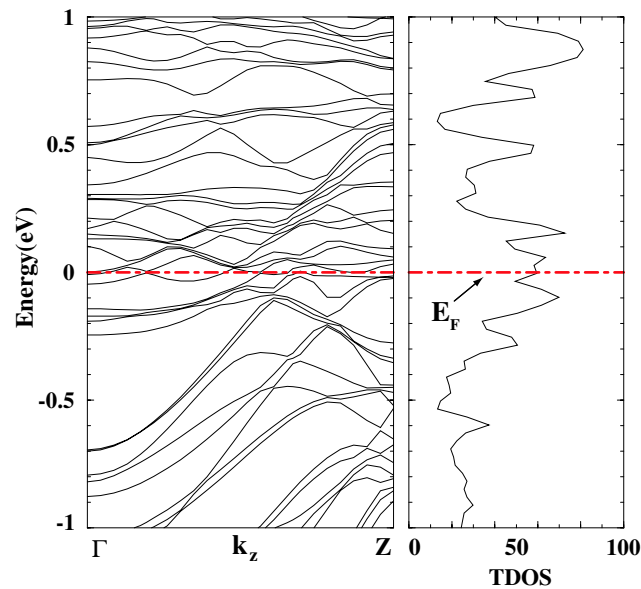


Figure 2. (a) Electronic energy band structure of a Ti covered (8,0) SWNT. (b) The total density of states (TDOS). TDOS of bare (8,0) tube is shown by dashed lines. Zero of energy is taken at the Fermi level.

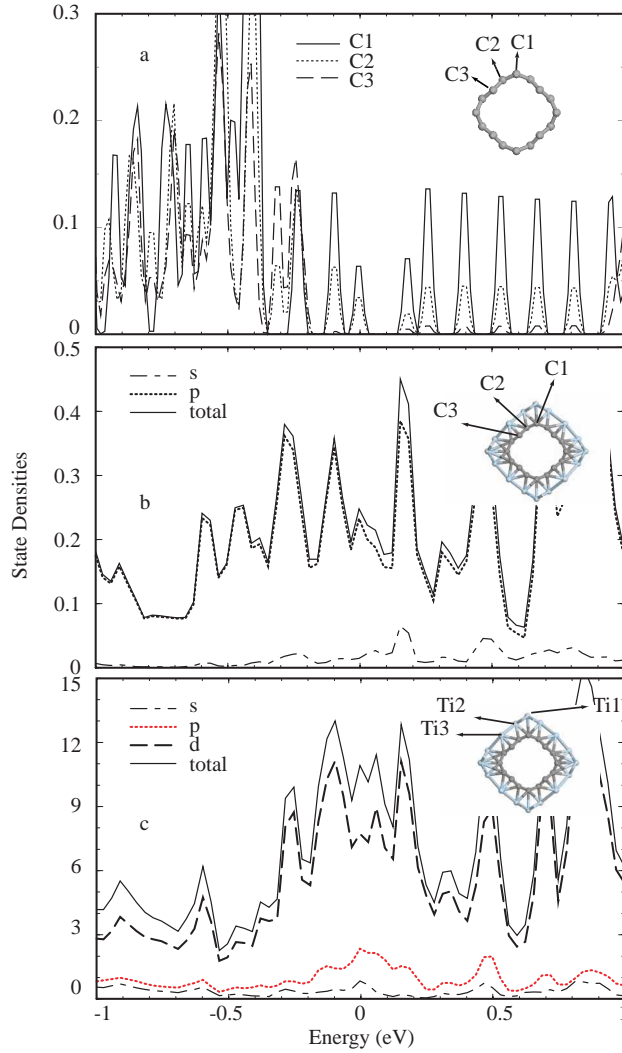


Figure 3. Calculated state densities. (a) Local density of states (LDOS) on C1, C2, C3 atoms of carbon nanotube which has the same atomic configuration and square-like cross section as the carbon nanotube covered by Ti as shown in Figure 1. See inset. (b) LDOS on the carbon atoms of the Ti covered SWNT (*i.e.* C1+C2+C3). (c) LDOS calculated on the Ti atoms of the Ti covered SWNT (*i.e.* Ti1+Ti2+Ti3). Partial density of states of *s*-, *p*-, and *d*-orbitals are also shown.

4. Effect of additional Ti atoms

We investigate now the effect of the adsorption of additional Ti atoms on (8,0) SWNT (*i.e.* $C_{32}Ti_{16}$) surface. Whether regular atomic structure and the electronic properties of $C_{32}Ti_{16}$ (Figure 4(a)) are affected will be the issue we shall clarify. To this end, we consider four additional Ti atoms are attached at the corners of the square-like cross section of $C_{32}Ti_{16}$ to make $C_{32}Ti_{20}$. The fully optimized, stable atomic structure of $C_{32}Ti_{20}$ is shown in Figure 4(d). The adsorption of four additional Ti atoms corresponds to the initial stage of second Ti atomic layer to cover SWNT surface. The average binding energy of these additional Ti atoms was found to be ~ 4.6 eV/atom. It is larger than that of $C_{32}Ti_{16}$ owing to the onset of Ti-Ti coupling in 3D. The effect of these four Ti atoms on the structure of $C_{32}Ti_{16}$ is minute. However, the calculated magnetic moment undergoes a dramatic change upon the chemisorption; μ of $C_{32}Ti_{16}$ decreases from $15.3 \mu_B/cell$ to $6.8 \mu_B/cell$ in $C_{32}Ti_{20}$. This important result implies that the net magnetic moment of Ti covered

SWNT is strongly dependent on the amount, as well as geometry of Ti coverage. The magnetization of the nanostructure $C_{4n}Ti_N$ can be engineered by varying the number N , and the decoration of adsorbed Ti atoms.

Spin polarized band structures for both geometries exhibited in Figure 4 (b) and (e) clearly indicate the metallic and high-conducting nature of both systems.

Densities of states corresponding to majority and minority spin states in Figure 4(c) and (f) indicate that $P(E_F)$ is low and hence $C_{32}Ti_{16}$ and $C_{32}Ti_{20}$ structures apart being high-conducting may not be of interest for spintronics applications.

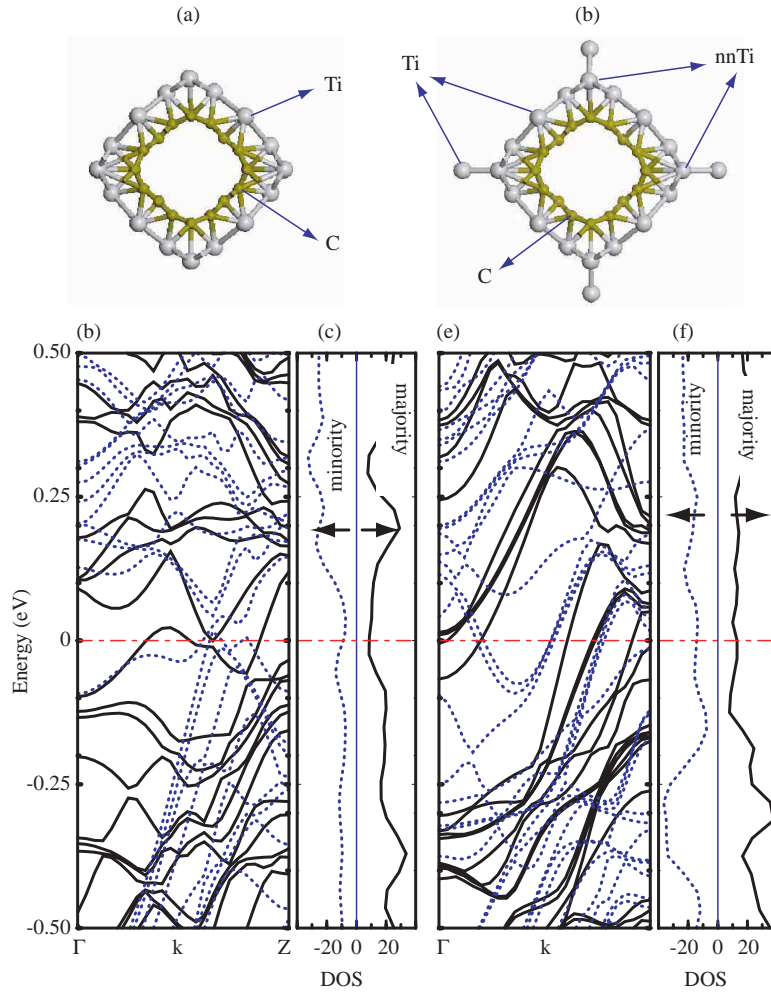


Figure 4. (a) Fully optimized atomic structure and square-like cross section of Ti coated (8,0) zigzag SWNT including 16 Ti atoms per unit cell ($C_{32}Ti_{16}$). Ti and C atoms are indicated by large-light and small-dark circles. (b) Spin-polarized band structure of $C_{32}Ti_{16}$ at $\epsilon_{zz} = 0$ with the Fermi level set to zero of energy. Majority spin, $E_n(\mathbf{k} \uparrow)$ and minority spin, $E_n(\mathbf{k} \downarrow)$ bands are shown by continuous and dotted lines, respectively. (c) Spin polarized density of states for majority $D^\uparrow(E)$ and minority $D^\downarrow(E)$ spin states. (d) Fully optimized atomic structure of Ti covered (8,0) SWNT including four additional Ti atoms adsorbed at the corners of the square-like tube (*i.e.* $C_{32}Ti_{24}$). (e) and (f) show corresponding spin-polarized band structure and DOS, respectively. Nearest Ti atoms to the four additional adsorbed Ti atoms are indicated by nnTi.

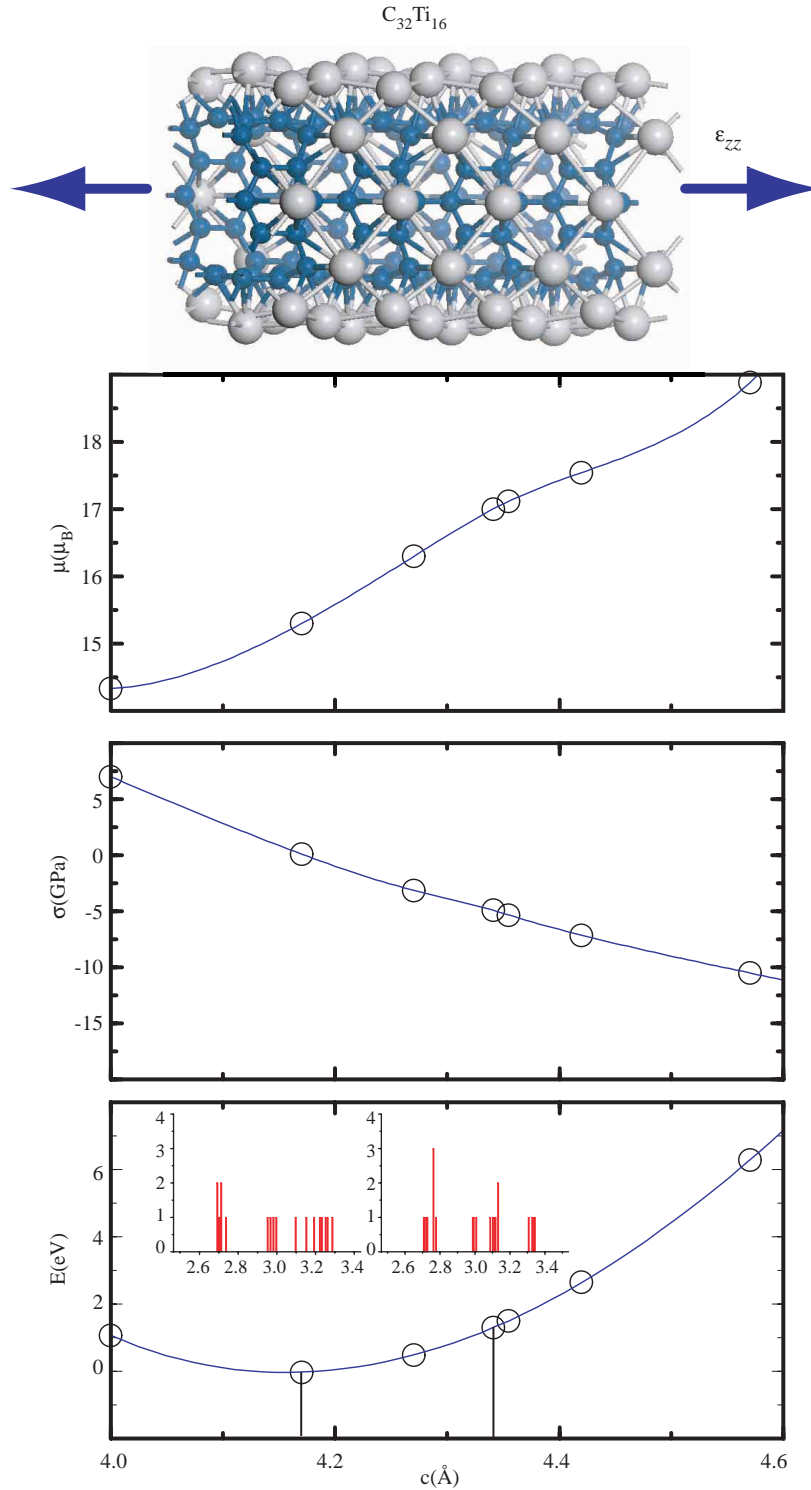


Figure 5. Top Inset: side view of the Ti covered (8,0) SWNT (*i.e.* $C_{32}Ti_{16}$) strained along its axis. $\epsilon_{zz} > 0$ corresponds to the stretched structure with $c > c_0$. (a) Variation of the magnetic moment μ per unit cell of $C_{32}Ti_{16}$ as a function of the lattice parameter c or strain. (b) Calculated axial stress in the system as a function of c . (c) Variation of the total energy E with c . The minimum of E occurs at $c_0 = 4.17 \text{ \AA}$. Insets in (c) show the distribution of Ti-Ti bond-lengths corresponding to $c_0 = 4.17 \text{ \AA}$ and $c = 4.34 \text{ \AA}$.

5. Effects of radial and axial strain

Present results indicate that the spin-dependent electronic structure and the magnetic moment of these nanostructures can be modified also by applied axial and radial strain, ϵ_{zz} . In Figure 5(a) the magnetization of a Ti covered (8,0) SWNT is plotted as a function of c . Each theoretical data point corresponds to the magnetic moment of $C_{32}Ti_{16}$ system relaxed under the constraint of a fixed c , hence under a given axial strain ϵ_{zz} . Figure 5(b) and 5(c) also show the change of stress and total energy as a function of c . The equilibrium lattice parameter occurs at $c_0 = 4.17 \text{ \AA}$. The axial strain is defined as $\epsilon_{zz} = (c - c_0)/c$. Starting from a compressive range with $\epsilon_{zz} < 0$, the net magnetic moment μ of $C_{32}Ti_{16}$ increases with increasing c , and continues to increase by stretching the system along the tube axis in the expansive range with $\epsilon_{zz} > 0$.

Ferromagnetism in magnetic structures is generally explained in terms of Heisenberg model which considers spin-spin coupling between magnetic atoms at different lattice sites through exchange interaction. First-principles calculations based on DFT, which treat the magnetism of metallic structures from the viewpoint of itinerant electrons reveal that a ferromagnetic state is energetically favorable. In fact, when c increases, average Ti-Ti distance will increase (see inset in Figure 5). Here parallel spin alignment is promoted by a $p-d$ hybridization, hence by electron transfer between the localized d orbitals of Ti atoms and extended $2p$ orbitals of C atoms. The important role of C atoms is also pointed out in recent DFT calculations [16], where p -orbitals of C are found to interact strongly with the d -orbitals of adsorbed Ti. The stronger the $p-d$ hybridization, the lower the $d-d$ exchange interaction and consequently resulting magnetic moment. Here increasing Ti-Ti distance decreases the $d-d$ coupling between Ti-Ti atoms, but increases the $p-d$ hybridization. The fact that in the absence of Ti-Ti coupling the magnetic moment of $C_{32}Ti_{16}$ could be sixteen times the magnetic moment of $C_{32}Ti$, *i.e.* $16 \times 2.2 \mu_B$ instead of $15.3 \mu_B$, corroborates our arguments.

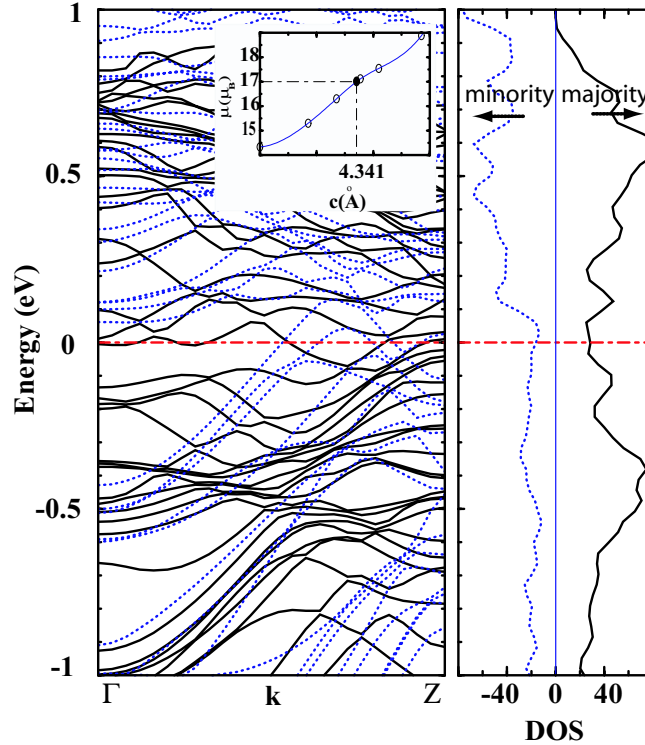


Figure 6. Calculated spin-polarized band structure of $C_{32}Ti_{16}$ under $\epsilon_{zz} = 0.04$ at $c = 4.34 \text{ \AA}$. $E_n(\mathbf{k} \uparrow)$ and $E_n(\mathbf{k} \downarrow)$ are shown by continuous and dotted lines, respectively. Corresponding densities of majority and minority spin states are shown in the panel on the right hand side.

The decrease of magnetic moment of $C_{32}Ti_{16}$ from $15.3 \mu_B$ to $6.8 \mu_B$ owing to the adsorption of four additional Ti atoms can be explained also by using similar arguments. In Figure 4(d), additional Ti atoms

adsorbed at the high curvature sites of square-like cross section of $C_{32}Ti_{16}$ affect the interaction between existing Ti atoms at their close proximity with nearest C atoms of SWNT. These Ti atoms are specified as nnTi atoms in Figure 4(d). Increasing coupling among Ti atoms by forming 3D-like Ti particles at the corners causes electronic charge which was donated to nearby C atoms to be back donated to nnTi atoms and hence to decrease the $p-d$ hybridization. A detailed charge density analysis show that the excess charge of ~ 0.3 electrons at each carbon atom interacting with nnTi atoms of $C_{32}Ti_{20}$ decreases to ~ 0.2 electrons upon the adsorption of four additional Ti atoms. At the end, nnTi atoms which initially carry majority spin as others, have their spin flipped upon the adsorption of additional Ti atom. This situation implies that the magnetic moment of Ti coated SWNT will decrease further as Ti coverage increases.

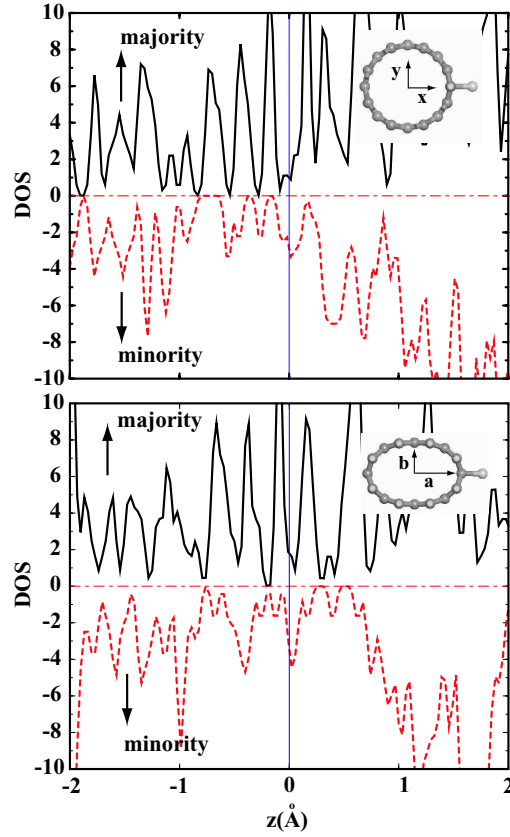


Figure 7. (Densities of majority and minority spin states of $C_{32}Ti$ showing curvature effect on $P(E)$. (a) Density of spin states for a single Ti atom adsorbed on a bare (8,0) SWNT. (b) Density of states for a single Ti atom adsorbed on the high curvature site of (8,0) SWNT under radial deformation $\epsilon_{yy} = 0.3$, which transforms the circular cross section to an elliptical one as shown by insets.

Half-metals [23, 24, 25] are another class of materials, which exhibit spin-dependent electronic properties relevant for spintronics. Half-metals, where the bands exhibit metallic behavior for one spin direction, but become semiconducting for the opposite spin-direction provide ultimate spin polarization of $P = 1$ at E_F . Accordingly, the difference between the majority and minority spin electrons per unit cell should be an integer number. Interestingly, as seen in Figure 5(a) the magnetic moment of $C_{32}Ti_{16}$ becomes equal to $17 \mu_B$ under the strain $\epsilon_{zz} \sim 0.04$ corresponding to $c = 4.34 \text{ \AA}$. An integer μ per unit cell reminds the possibility of a half-metallic behavior. In Figure 6 the band structure and DOS of $C_{32}Ti_{16}$ corresponding to $\epsilon_{zz} \sim 0.04$ are illustrated. Here, since both $E_n(\mathbf{k} \uparrow)$ and $E_n(\mathbf{k} \downarrow)$ cross the Fermi level, the system is a ferromagnetic metal, but $P(E_F)$ is significantly increased as compared to the case of $\epsilon_{zz} = 0$ shown in Figure 4(b). Hence, whereas the half-metallic behavior did not occurred, the spin-polarization has been enhanced significantly and becomes suitable for spintronic applications. The analysis of spin-polarized bands

of $C_{32}Ti_{16}$ for $c_0 = 4.17 \text{ \AA}$ and $c = 4.34 \text{ \AA}$ shows that in the later 64% (36%) of the current is carried by majority (minority) spin states. Whereas, in the case of $c_0 = 4.17 \text{ \AA}$ (*i.e.* $\epsilon_{zz} = 0$) the shares of majority and minority spins are almost equal. This is clearly another interesting effect of applied strain.

Finally, we explore the effect of radial strain $\epsilon_{yy} = (b - R)/R$, which is defined in terms of the minor, b and major, a axis of the elliptically deformed cross section and the radius R of the bare tube. Earlier studies have revealed important effects of the radial deformation of SWNTs on their electronic and chemical properties [26, 27]. For example a sSWNT has become metallic and electronic charge distribution on its surface has undergone a significant change. It has been also found that the chemical activity of SWNT at the high curvature site has increased to lead to a stronger bonding with foreign atoms such as H, Al [28]. Here we expect that the spin-dependent electronic structure of Ti adsorbed on SWNT is affected by radial deformation. In Figure 7, we show the calculated $D^\uparrow(E)$ and $D^\downarrow(E)$ of the $C_{32}Ti$, where Ti is adsorbed on the bare, as well as at the high curvature site of a radially deformed ($\epsilon_{yy} \sim 0.3$) (8,0) SWNT. Radial deformation had minute effect to the value of net magnetic moment. However, the dispersion of bands and $P(E)$ near E_F have been affected by radial deformation. The forms of $D^\uparrow(E)$ and $D^\downarrow(E)$ near E_F suggest that the spin-dependent transport under bias voltage V_b can be monitored by ϵ_{yy} .

6. SWNT with different radius and chirality

Finally, we demonstrated that the uniform coverage of Ti resulting in a regular atomic structure occurs also for SWNTs with different radius and chirality. Figure 8 shows the optimized atomic structure of Ti covered (9,0) zigzag and (6,6) armchair tubes. The former bare tube has a very small band gap of 0.09eV, radius of 3.6 \AA and odd number of C atoms on the circumference. The latter tube is a metal and has radius of 4.1 \AA and chiral angle of 30° when it is free of Ti. However, both tubes become metal with high $\mathcal{D}(E_F)$ and have magnetic ground state upon coverage with Ti. The calculated magnetic moments are $3.5 \mu_B$ and $4.4 \mu_B$ for (9,0) and (6,6) SWNTs, respectively. Sharp corners of the square-like cross section in Figure 1 start to be flattened and change to polygonal form for the Ti covered (6,6) SWNT.

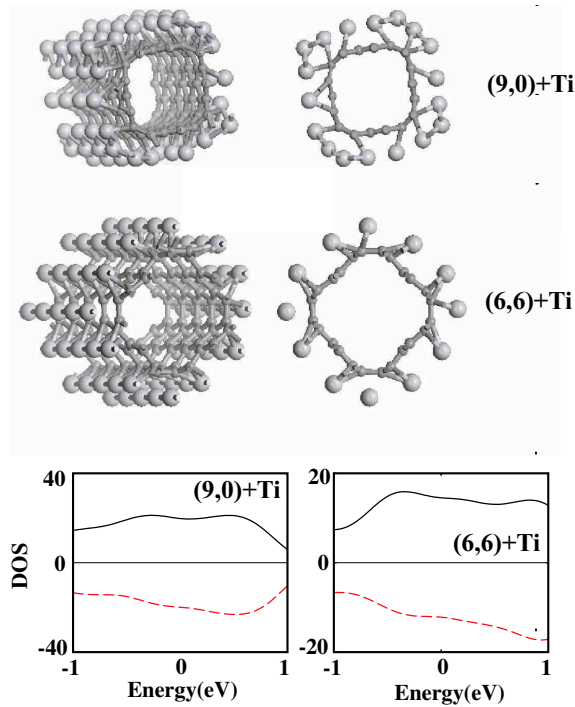


Figure 8. Optimized atomic structure of (9,0) zigzag and (6,6) armchair SWNT which are covered with Ti. Corresponding density of states for spin-up and spin-down electrons are shown.

7. Conclusions

First principles, spin-relaxed calculations showed that the chemical interaction between SWNTs and Ti atom adsorbed to the hollow site is significant and favors the continuous coating of the tube surface. Depending on the radius and the chirality the circular cross section changes to either square like or polygonal form. A semiconducting SWNT is metallized upon the adsorption of Ti atoms. Zigzag, as well as armchair SWNTs are metallic and have ferromagnetic ground state when they are continuously covered with Ti atoms. Spin-relaxed calculations predict interesting spin-dependent electronic and magnetic properties. The magnetic moment of the (8,0) SWNT can increase with increasing number of adsorbed Ti atoms to a value as large as $15.3 \mu_B$; it, however, decreases if additional Ti atoms are adsorbed on the Ti coating covering on SWNT surface. We showed that the magnetic properties of the Ti covered SWNT can be modified also by applied axial strain; the magnetic moment increases with increasing ϵ_{zz} (namely by stretching the tube). Not only net magnetic moment, but also the spin-polarization at the Fermi level can be increased by increasing axial strain. Finally, we studied the effect of the radial strain on the spin-dependent electronic and magnetic properties. We found the dispersion of the spin-dependent bands and resulting density of states near the Fermi level of a single Ti-atom-adsorbed (8,0) SWNT is modified upon radial deformation. We expect that these coverage and strain dependent electronic and magnetic properties of Ti coated SWNTs can lead to interesting applications in spintronics and nanoscale magnetism.

Acknowledgements

Part of computation for the work described in this paper was supported by TUBITAK ULAKBIM High Performance Computing Center. SC acknowledges partial financial support from Academy of Science of Turkey.

References

- [1] H. Ohnishi, Y. Kondo, and K. Takayanagi, *Nature* (London), **395**, (1998), 783.
- [2] A. I. Yanson, G. R. Bollinger, H. E. Brom, N. Agraït, and J. M. Ruitenbeek, *Nature* (London), **395**, (1998), 783.
- [3] N. Agraït, G. Rubio, and S. Vieira, *Phys. Rev. Lett.*, **74**, (1995), 3995.
- [4] S. Ciraci, E. Tekman, *Phys. Rev. B*, **40**, (1989), 11969; E. Tekman and S. Ciraci, *Phys. Rev. B*, **43**, (1991), 7145; H. Mehrez, S. Ciraci, A. Buldum, and I.P. Batra, *Phys. Rev. B*, **55**, (1997), R1981.
- [5] S. Ciraci, A. Buldum, and I.P. Batra, *J. Phys.: Condens. Matter*, **13**, (2001), R537.
- [6] A. Buldum, S. Ciraci, C. Y. Fong, *J. Phys.: Condens. Matter*, **12**, (2000), 3349 ; A. Buldum, D. M. Leitner, and S. Ciraci, *Europhys. Lett.*, **47**, (1999), 208; A. Ozpineci and S. Ciraci, *Phys. Rev. B*, **63**, (2001), 125415 .
- [7] H. Dai, E. W. Wong, Y. Z. Lu, S. Fan, and C. M. Lieber, *Nature* (London), **375**, (1995), 769 ; W. Q. Han, S. S. Fan, Q. Q. Li, and Y. D. Hu, *Science*, **277**, (1997), 1287.
- [8] Y. Zhang and H. Dai, *Appl. Phys. Lett.*, **77**, (2000), 3015 ; Y. Zhang, N.W. Franklin, R.J. Chen, and H. Dai, *Chem. Phys. Lett.*, **331**, (2000), 35.
- [9] C. Zhou, J. Kong, and H. Dai, *Phys. Rev. Lett.*, **84**, (2000), 5604.
- [10] M. C. Payne, M. P. Teter, D. C. Allen, T. A. Arias, and J. D. Joannopoulos, *Rev. Mod. Phys.*, **64**, (1992), 1045.
- [11] G. Kresse and J. Hafner, *Phys. Rev. B*, **47**, (1993), 558 ; G. Kresse and J. Furthmüller, *ibid*, **54**, (1996), 11169.
- [12] P. Hohenberg and W. Kohn, *Phys. Rev.*, **136**, (1964), B864; W. Kohn and L. J. Sham, *Phys. Rev.*, **140**, (1965), A1133.
- [13] J. P. Perdew, J. A. Chevary, S. H. Vosko, K. A. Jackson, M. R. Pederson, D. J. Singh, and C. Fiolhais, *Phys. Rev. B*, **46**, (1992), 6671.

- [14] D. Vanderbilt, *Phys. Rev. B*, **41**, (1990), 7892.
- [15] H.J. Monkhorst and J.D. Pack, *Phys. Rev. B*, **13**, (1976), 5188.
- [16] E. Durgun, S. Dag, V.K. Bagci, O. Gülseren, T. Yildirim, and S. Ciraci, *Phys. Rev. B*, **67**, (2003), R201401.
- [17] C.C. Kaun, B. Larade, H. Mehrez, J. Taylor, and H. Guo, *Phys. Rev. B*, **65**, (2002), 205416.
- [18] B. L. Altshuler and A. G. Aronov in *Electron-electron interaction in disordered systems*, Eds: A. L. Efros and M. Pollak, Elsevier Amsterdam (1985).
- [19] X. Blase, L.X. Benedict, E.L. Shirley, and S.G. Louie, *Phys. Rev. Lett.*, **72**, 1994, 1878.
- [20] C. Kilic, S. Ciraci, O. Gülseren, and T. Yildirim, *Phys. Rev. B*, **62**, (2000), 16345.
- [21] O. Gülseren, T. Yildirim, and S. Ciraci, *Phys. Rev. Lett.*, **87**, (2001), 116802.
- [22] O. Gülseren, T. Yildirim, and S. Ciraci, *Phys. Rev. B*, **68**, 115419, (2003).
- [23] S. A. Wolf, D. D. Awschalom, R. A. Buhrman, J. M. Daughton, S. von Molnár, M. L. Roukes, A. Y. Chtchelkova, and D. M. Treger, *Science*, **294**, (2001), 1488.
- [24] R. A. de Groot, F. M. Mueller, P. G. van Engen, and K. H. J. Bushkow, *Phys. Rev. Lett.*, **50**, (1983), 2024.
- [25] W.E. Pickett and J.S. Moodera, *Phys. Today* **54**, (2001), 39.
- [26] S. Ciraci, S. Dag, T. Yildirim, O. Gülseren, and T. Senger, *J. Phys.: Condens. Matter*, **16**, (2004), R901.
- [27] C. Kilic, S. Ciraci, O. Gülseren and T. Yildirim, *Phys. Rev. B*, (2000), R16345.
- [28] O. Gülseren, T. Yildirim, and S. Ciraci, *Phys. Rev. Lett.*, **87**, (2001), 116802.